Molecular BioSystems

Cite this: *Mol. BioSyst.*, 2011, **7**, 1564–1575

www.rsc.org/molecularbiosystems

PAPER

Synthesis and evaluation of conformationally restricted inhibitors of aspartate semialdehyde dehydrogenase†

Andrew S. Evitt*[a] and Russell J. Cox*[b]

Received 7th October 2010, Accepted 9th February 2011
DOI: 10.1039/c0mb00227e

Inhibitors of the enzyme aspartate semialdehyde dehydrogenase, a key biological target for the generation of a new class of antibiotic compounds, have been developed. To investigate improvements to binding within an inhibitor series, the lowering of the entropic barrier to binding through conformational restriction was investigated. A library of linear and cyclic substrate analogues was generated and computational docking used to aid in structure selection. The cyclic phosphonate inhibitor **18** was thus identified as complimentary to the enzyme active-site. Synthesis and *in vitro* inhibition assay revealed a K_i of 3.8 mM against natural substrate, where the linear analogue of **18**, compound **15**, had previously shown no inhibitory activity. Two further inhibitors, phosphate analogue diastereoisomers **17a** and **17b**, were synthesised and also found to have low millimolar K_i values. As a result of the computational docking investigations, a novel substrate binding interaction was discovered: hydrogen bonding between the substrate (phosphate hydroxy-group as the hydrogen bond donor) and the NADPH cofactor (2′-oxygen as the hydrogen bond acceptor).

Introduction

The aspartate biosynthetic pathway is responsible for the production of four essential amino acids (threonine, isoleucine, methionine and lysine) and important primary metabolites such as diaminopimelate (DAP) **4** in bacteria (Scheme 1).[1,2] The pathway is not found in mammals but is critical to the survival of bacteria and thus presents a potential target for novel antimicrobial agents. The aspartate pathway is not targeted by the current generation of clinical antibacterial agents and inhibition of the pathway would be expected to overcome the resistance that is now undermining last-line-of-defense medicines.[3]

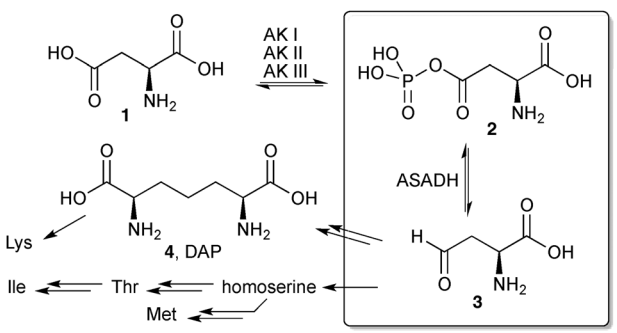

Scheme 1 Key transformations of the aspartate pathway. AK = aspartokinase.

Aspartate semialdehyde dehydrogenase (ASADH, EC 1.2.1.11) is found immediately prior to the first branch-point in the aspartate pathway. Unlike the enzymes found in the catalytic steps surrounding ASADH there are no analogous enzymes that can replace the catalytic function of ASADH, marking ASADH as a unique weak-point in the pathway.[1] The vital role of ASADH in bacteria has been demonstrated through the creation of *Salmonella enterica* mutants deficient in the *asd* gene encoding ASADH.[4] Mutants lacking *asd* are auxotrophic for diaminopimelate **4** and lysine, chemicals which are required for the construction of the peptidoglycan layer of the bacterial cell wall.[5] Furthermore, genetic deficiency in ASADH has been used as a strategy for the creation of successful vaccine strains of *Salmonella typhimurium*, *Streptococcus mutans* and *Legionella pneumophila*.[6–8] By preventing ASADH function instead through the mechanism of potent selective small-molecule inhibitors, it is expected to obtain lethality towards bacteria without side-effects in mammals.

The mechanism of ASADH is well understood, particularly through comparisons to extensively studied enzymes such as serine proteases and the highly analogous 3-phospho-glyceraldehyde dehydrogenase.[9–13] In the biosynthetic (dephosphorylating) direction, the thiol of C135 (*E. coli* numbering) is deprotonated by H274 to generate an ionic pair (Scheme 2).

[a] *Pharmaceutical Science Division, King's College London, Franklin-Wilkins Building, 150 Stamford Street, London, UK, SE1 9NH*
[b] *School of Chemistry, University of Bristol, Cantock's Close, Bristol, UK, BS8 1TS*
† Electronic supplementary information (ESI) available: See DOI: 10.1039/c0mb00227e

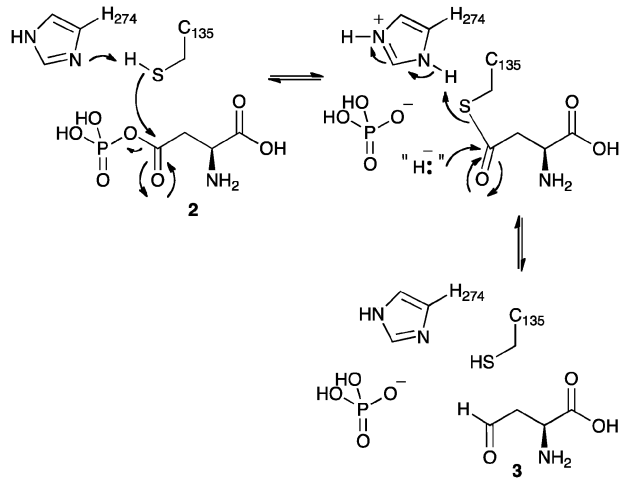

Scheme 2 Simplified mechanism of ASADH.

The C135 thiolate then attacks the β-carbonyl of β-aspartyl-phosphate (BAP, **2**) giving a tetrahedral oxyanion that is likely stabilised by N135.[9] Collapse of the tetrahedral intermediate expels phosphate to generate the enzyme-bound thiolester intermediate. The thiolester is reduced by hydride transfer from NADPH, proceeding through a second stabilised tetrahedral intermediate to release the product aspartate semialdehyde (ASA **3**), inorganic phosphate (P_i) and $NADP^+$ (Scheme 2). Kinetic studies have shown that the order of binding/release for BAP/NADPH is random and ASA/P_i/$NADP^+$ proceeds with a non-obligatory preference for P_i and $NADP^+$ to bind before or release after ASA.[14] NADP(H) and P_i are bound to the enzyme during the steps in which they are required but it has been noted that NADPH remains bound throughout the phosphate thiolysis stage and that P_i remains bound throughout the hydride transfer stage, steps for which they are respectively not required.

The previously designed ASADH inhibitors possessed low millimolar inhibition constants (Fig. 1).[15,16] The reason

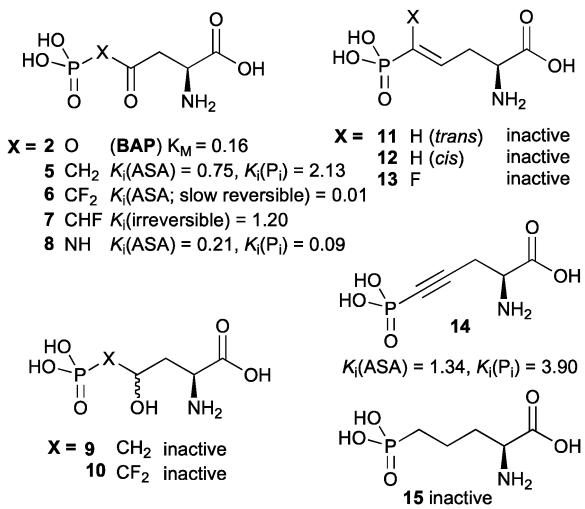

Fig. 1 The natural substrate (BAP, with K_M value) and previous inhibitors (with K_i values; all values in mM).[15,16] K_i values for both ASA and inorganic phosphate (P_i) represent competitive inhibitors. Remaining compounds noted as irreversible inhibitors or inactive as inhibitors.

underlying why the inhibition constants are not appreciably lower than the K_M value of BAP **2** potentially arises from their structural similarity—inhibitor binding was most likely mirroring the binding of BAP. This theory is further supported by the fact that the inhibition was competitive. To further improve binding, and thus inhibition, we decided to pursue a strategy of reducing the entropic cost of binding through conformational restriction. Conformational restriction has proven to be a useful strategy in certain classes of inhibitor, showing for example over 400-fold improvement to binding upon cyclisation of pentapeptide inhibitors of penicillopepsin, an aspartate protease.[17] Cyclisation of inhibitor structures would also provide a carbon framework upon which to build further functionality complimentary to the enzyme active-site, providing the potential for furthering the enthalpic benefit to binding.

Computational docking

To select inhibitor structures that were complimentary to the active-site of ASADH, computational simulated docking was employed.

Selection of ASADH coordinate file

Computational simulated docking was performed using the FlexX software package (BioSolveIT GmbH)[18] which requires a rigid enzyme file, the coordinates of which are held constant through the computation. Five ASADH coordinate sets were selected from the RCSB protein databank in order to study the suitability of applying a rigid structure simulated docking method to ASADH (Fig. 2). The sequences were chosen for

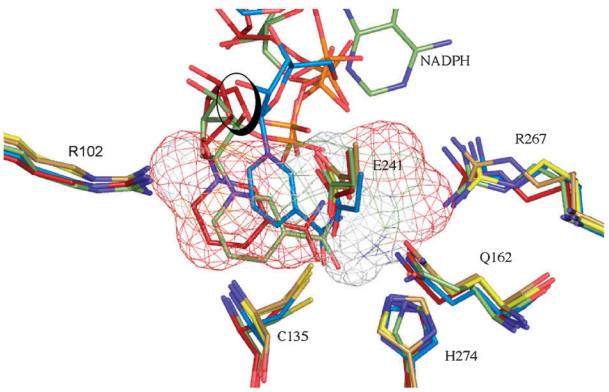

PDB code	Microbial Host	Ligands	Identity[a]
1GL3 (green)	*E. coli*	NADPH, SMCS[b]	100
1T4B (brown)	*E. coli*	*apo*	99
1NWH (yellow)	*H. influenzae*	NADPH, ASA	72
2GZ3 (red)	*S. pneumoniae*	*apo*	24
1YS4 (blue)	*M. jannaschii*	NADPH	12

Fig. 2 Comparison of ASADH coordinate sets from the RSCB protein databank. A low overall sequence identity does not affect the active site sequence and structural identity. Highlighted: the 2′OH groups of the NADPH ribose locate within 1.4 Å despite greater distances in the remainder of the NADPH molecule. Mesh depicts the binding pocket occupied by substrate. [a]Sequence identity calculated using ClustalW2. [b]SMCS: *S*-methyl cysteine sulfoxide.

their diversity of source microbe: Gram negative *E. coli* (1GL3 and 1T4B), Gram negative *H. influenzae* (1NWH), Gram positive *S. pneumoniae* (2GZ3) and the archaea *M. jannaschii* (1YS4). The overall sequence identity of ASADH varied between 72% (1GL3 against 1NWH) and 12% (1GL3 against 1YS4), correlating with phylogenetic separation (ClustalW2 alignment of all sequences in ESI†).

Despite overall sequence identities as low as 12%, the sequence and the structure of residues within the active-site were observed to be near identical (Fig. 2). The NADPH cofactor overlaid less reproducibly, although the active hydride and 2′OH resided in similar spatial positions. The coordinate set 1GL3 was selected for the simulated docking studies as this structure contains the cofactor NADPH and is from the *E. coli* isoform of ASADH, which we use for *in vitro* inhibition studies.

The charge states of the enzyme active-site residues were set automatically by the FlexX algorithm. The protonation states of the catalytic dyad residues, C135 and H274, were investigated through manual modification and assessment by simulated docking (ESI† Fig. 2). It was found that C135 SH torsion angles and H274 conformation did not affect results significantly, but that better results were observed when C135–H274 were set as the charged pair (*i.e.* C135 anion, H274 cation).

The docking results were examined by compiling an overlay of the top scoring poses. For tightly binding ligands the top scoring poses should lie in a narrow area of the orientation space and therefore overlay well (seen, for example, in Fig. 3a and d) while for a weakly binding structure the top scoring poses would be spread more widely across the orientation space (seen, for example, in Fig. 3c).

BAP docking

Initial simulated docking experiments were performed on the natural substrate BAP **2** in order to examine performance of the docking software. While the exact binding mode of **2** has not been observed crystallographically, many key interactions have been elucidated from site-directed mutagenesis and intermediate-trapping experiments,[9] and the simulated docking results matched these interactions (Fig. 3a). In particular, the BAP backbone was stretched between arginine residues R102 and R267, with the phosphate functional group in contact with R102 and the carboxylate with R267. The protonated amine located in a pocket of hydrogen bond acceptors (1.5 Å to E241, 2.0 Å to Q162 and 2.2 Å to C135) and the substrate carbonyl located within 4 Å of the C135 active-site nucleophile.

During these simulated docking studies, the protonation states of the BAP substrate were set as the charged carboxylate and ammonium groups. Analysis of the pK_a of the phosphate group suggested that the first proton would be absent under physiological conditions (pK_{a1} = 1.5–2.0) but the second protonation state remained in question (pK_{a2} = 6.5–7.0).[19] All three possible protonation states of the phosphate were therefore examined in separate experiments by simulated docking. Full protonation led to a loss of interaction with R102 while full deprotonation maintained good binding with R102. Single protonation, however, led to electrostatic binding with R102 and formation of a hydrogen bond between the BAP phosphate (acting as the hydrogen bond donor) and the NADPH ribose 2′OH (hydrogen bond acceptor, Fig. 3a and b).

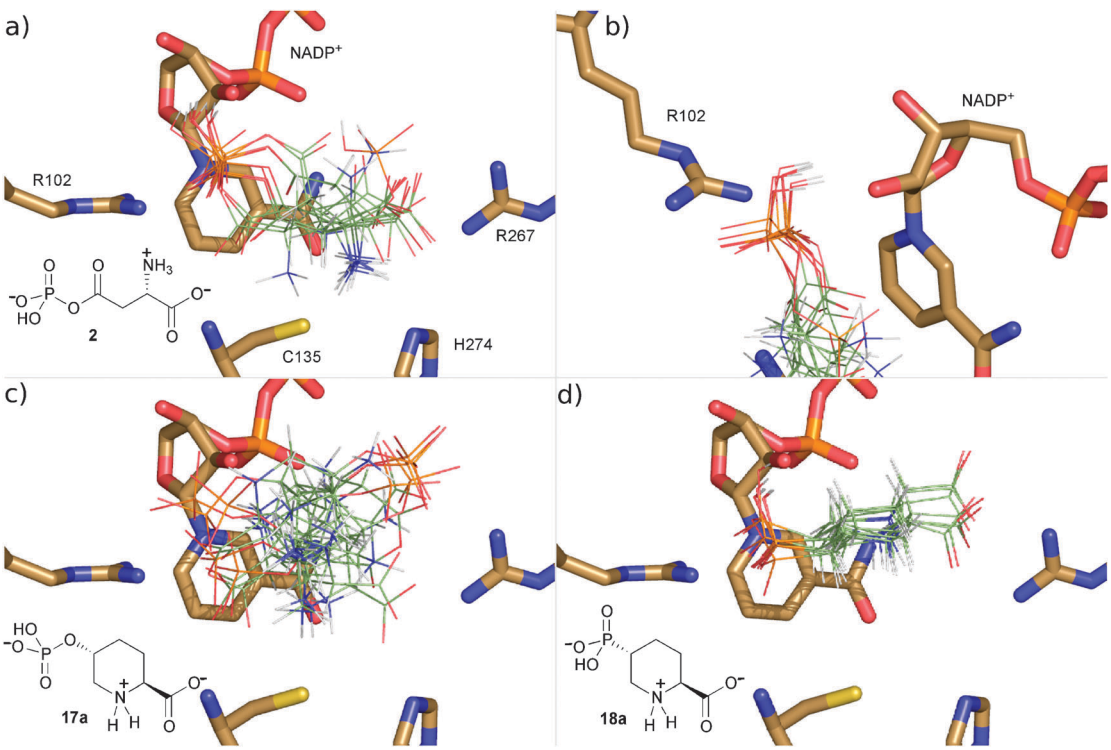

Fig. 3 The results of computational docking presented as overlays of the top scoring poses; (a) natural substrate BAP **2**; (b) BAP, highlighting the hydrogen-bond between the substrate phosphate and $NADP^+$; (c) poor alignment of putative phosphate inhibitor **17a**; (d) good alignment of putative phosphonate inhibitor **18a**.

Without a hydrogen bond between substrate and NADPH the alignment, and hence overall binding of substrate, was adversely affected (ESI† Fig. 3 and 4).

A study of all the available coordinate files in the RSCB protein databank revealed that no examples where the NADPH 2′OH acts as the hydrogen bond acceptor have previously been reported. Three examples were found demonstrating that the NADPH ribose 2′OH can act as the hydrogen bond donor.[20–22] Simulated docking was therefore used to investigate the NADPH 2′OH as the hydrogen bond donor, which was performed by rotating the 2′OH torsion so that the oxygen lone pairs were directed towards the phosphate binding site. This led to complete loss of the hydrogen bond, indicating that the 2′OH in ASADH-bound NADPH cannot act as the hydrogen bond donor (data not shown). As a result of these experiments, the phosphate moiety was consistently set as singly deprotonated in all following docking experiments. After highlighting theoretical strongly-binding structures, determining if single deprotonation under physiological conditions is likely for that structure would be performed.

Library docking

A virtual compound library totaling 182 structures was created, encompassing the natural substrate, previous inhibitors,[15,16] a series of putative linear and cyclic (5-, 6-, and 7-membered rings) BAP analogues, all bearing functional groups in a wide variety of locations and stereochemistries (depicted in Fig. 4 and set out in full in ESI† Fig. 5). The amine and carboxylic acid groups were set as charged and the phosphate groups were set as singly deprotonated. This library was submitted to FlexX and the results were assessed by visual inspection of binding interactions and then further by overlay assessment as described for the natural substrate.

The results revealed that several of the 5- and 7-membered rings could form favourable interactions with the active-site, but it became apparent that the goodness-of-fit arose from the flexibility available to these ring sizes. The 5-membered rings took advantage of choice of puckered ring atom (ESI† Fig. 6) and the 7-membered rings could sample a wide range of conformations simply due to their size (ESI† Fig. 7). The lack of conformational restriction observed in the 5- and 7-membered ring inhibitors led us to believe that binding would not be improved as there would be little reduction in entropy. Efforts were therefore focused on the 6-membered rings, which are restricted largely to one of the two conformers of the chair form. From the results of the 6-membered ring structures the functionalised pipecolate derivative **18a** was highlighted as complementary to the ASADH active site (Fig. 3d). Furthermore, pipecolate **18a** represents a

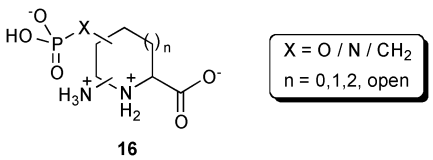

16

Fig. 4 Template for the creation of cyclic inhibitor library. All possible stereoisomers were automatically investigated.

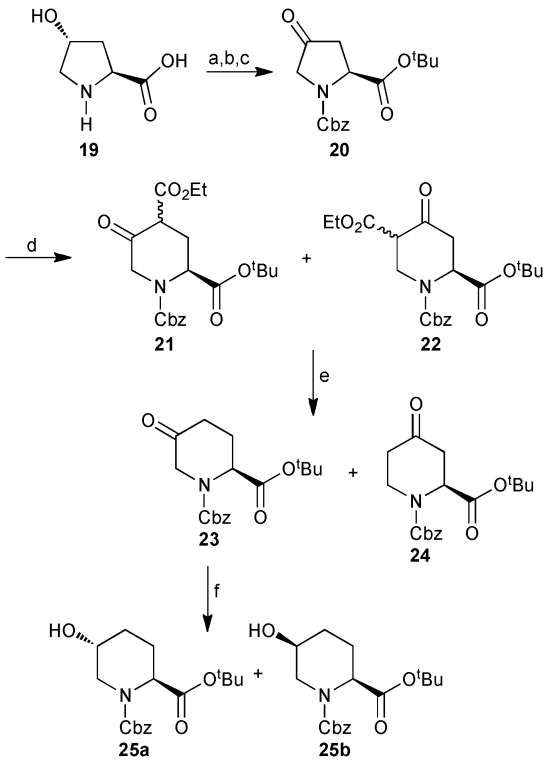

Scheme 3 *Reagents and conditions*: (a) TMS-Cl, DIPEA, DCM, reflux 2 h then Cbz-Cl, 0 °C to rt, 16 h, quant.; (b) Jones reagent, acetone, 0 °C, 10 min, 75%; (c) isobutylene, H_2SO_4 (cat.), CH_2Cl_2, rt, 16 h, 73%; (d) ethyl diazoacetate, $BF_3{\cdot}Et_2O$, Et_2O, rt, 1 h, 79%; (e) NaCl, DMSO, H_2O (cat.), 140 °C, 4 h, **23** in 34% and **24** in 36%; (f) L-selectride, THF, −45 °C to rt, 30 min, **25a** in 22% and **25b** in 40%.

structurally restrained analogue of **15**, a compound that had previously shown no inhibitory activity and therefore provides a platform on which to examine the effects of cyclisation. In a similar fashion to the natural substrate, pipecolate **18a** was located between R102 and R267, with the phosphate and carboxylate groups aligning in an analogous manner to **2**. The protonated ring amine of **18a** was well conserved throughout the overlaid poses but could not get as close to the E241–Q162–C135 hydrogen bonding pocket as the natural substrate amine, presumably owing to the conformational restriction within the parent structure. The protonated hydroxy-group of the phosphate was again observed to form a hydrogen-bonding interaction with the NADPH cofactor.

The proposed synthetic route to compound **18a** (*vide infra*) would also allow for rapid access to the structurally similar phosphate **17a**, and therefore this compound was also subjected to the simulated docking study (Fig. 3c). **17a** did not perform well in the docking study—the top scoring poses of **17a** did stretch the carboxylate and phosphate between the two arginine residues of the active site, but were often misaligned so that the inhibitor was inverted (*i.e.* the carboxylate formed interactions with R102 rather than R267). It was also noted that the amine does not make any consistent contact. We thus decided to synthesise and examine the phosphate inhibitor **17a** *in vitro* as a control for the reliability of the docking software.

Synthesis

The synthetic procedure of Jung and Avery[23] was exploited to rapidly access ketone **23** and diastereomeric alcohols **25a** and **25b** (Scheme 3).

Thus, *trans*-L-hydroxy proline **19** was protected and the hydroxyl group oxidised to give ketone **20**. Ring expansion with ethyl diazoacetate gave the regioisomeric pipecolate derivatives **21** and **22** which were not separated. The mixture was decarboxylated under Krapcho conditions[23] and the regioisomeric ketones **23** and **24** then separated by chromatography. We obtained a 15% overall yield of ketone **23** in comparison to Jung and Avery's 28%. Jung and Avery then screened a number of reducing agents showing that the stereoselective synthesis of the *cis* alcohol **25b** was possible through simply using sodium borohydride. As we required the *trans* diastereoisomer **25a** we made use of the reported sterically hindered reducing agent L-selectride, achieving a ratio of 1 : 2 **25a** : **25b** in 62% yield (Jung and Avery report a 2 : 3 ratio of **25a** : **25b** in 92% yield).

Reaction of the separate diastereomeric alcohols with dibenzyl iodophosphonate **26**, followed by full deprotection gave the phosphate inhibitors **17a** and **17b** as their HCl salts (Scheme 4). It was noted that the *cis*-phosphate **17b** was stable, while the *trans*-phosphate **17a** decomposed appreciably over 72 h and thus was assayed immediately after preparation.

For synthesis of phosphonate **18a**, the main target highlighted in the docking study, a method of constructing a secondary carbon to phosphorus bond was required. The lack of a general procedure for bond formation between secondary carbons and phosphorus, coupled with the great deal of steric bulk inherent in the cyclohexyl system, indicated a challenging synthetic conversion. A great deal of effort was invested into constructing this carbon–phosphorus bond, including the use of Michaelis–Arbuzov,[24,25] Michaelis–Becker,[26] Michaelis–Becker with Salvatore modification,[27] Perkow,[28] and chlorophosphonium techniques,[29] but all failed to produce the desired material. Thioketone methodology reported by Yoshida finally allowed access to these compounds (Scheme 5).[30,31] The protected pipecolate-5-ketone **23** was reacted with H_2S in a procedure reported to generate the geminal dithiol.[32] It was found, however, that a mixture comprising of the enethiol **28** and thioketone trimer **29** was obtained, but that this mixture underwent the desired reaction when refluxed with trimethylphosphite to generate a 2 : 1 mixture of pipecolate derivatives **30a** and **30b**. The thioether groups were removed by hydrogenolysis to give compound **32**, but this also led to partial cleavage of the Cbz group, giving compound **31**. Re-attachment of the Cbz group aided purification by chromatography and increased the isolated yield of the reaction. Full deprotection then led to the mixture of *trans*- and *cis*-diastereoisomers **18a** and **18b**. ^{1}H-NMR confirmed that the 2 : 1 ratio of *trans*- to *cis*-isomers that was set in the trimethylphosphite addition had been conserved throughout the deprotection, and the mixture of diastereoisomers was subjected to the inhibition study.

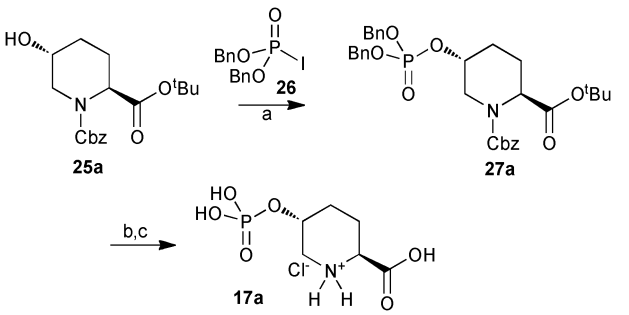

Scheme 4 *Reagents and conditions*: (a) pyridine, CH_2Cl_2, **26** (0.18 M in CH_2Cl_2), −20 °C to rt, 2 h, 60%; (b) TFA : DCM (1 : 1), 2 h, 84%; (c) H_2, Pd/C (10%), EtOH, 20 h, $HCl_{(aq)}$, 49%. **25b** was reacted using the same conditions in (a) 65%; (b) 60% and (c) 76% yield.

Inhibition assay

The procedure of Cox *et al*. was used to investigate inhibition of ASADH *in vitro*,[15] with the modification that bicine buffer was used in order to minimise imine formation between buffer and ASA. In brief, the ASADH-catalysed reaction was run in

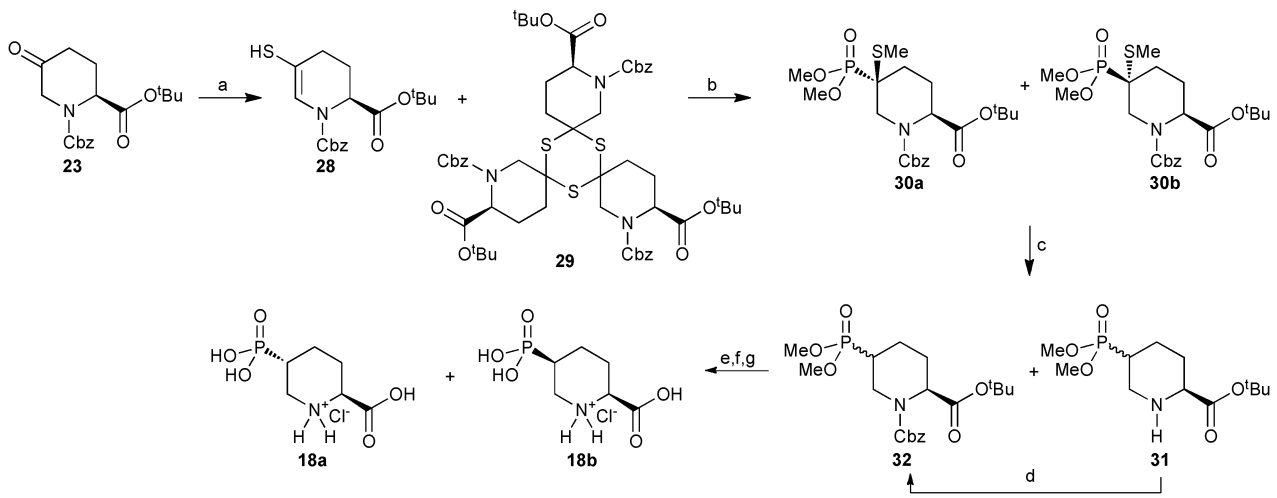

Scheme 5 *Reagents and conditions*: (a) H_2S, morpholine (0.1 eq), DMF, 10 °C, 5 h, **28** in 6%, **29** in 49%; (b) $P(OMe)_3$, toluene, reflux, 40 h, **30a** : **30b** 2 : 1, 67%; (c) Raney nickel, EtOH, 2 h; (d) DIPEA, Cbz-Cl, 0 °C to rt, 20 min, **32a** : **32b** 2 : 1, 79%; (e) 1 : 1 TFA : CH_2Cl_2, 2 h, 2 : 1 *trans* : *cis*, 96%; (f) Pd/C (10%), EtOH, 20 h, 2 : 1 *trans*:*cis*, 71%; (g) HCl (6 N), reflux, 5 h, **18a** : **18b** 2 : 1, 63%.

Table 1 Constants determined during kinetic investigations of ASADH

Kinetic parameter	ASADH
k_{cat}/s^{-1}	48.5 ± 6.4
K_M of ASA/mM	0.17 ± 0.03
K_M of P_i/mM	0.032 ± 0.013
k_{cat}/K_M of ASA/M^{-1} s^{-1}	$2.36 \times 10^5 \pm 1.07 \times 10^5$
k_{cat}/K_M of P_i/M^{-1} s^{-1}	$2.65 \times 10^5 \pm 0.77 \times 10^5$

reverse using synthetic ASA **3** as the substrate and $NADP^+$ as the cofactor. The initial velocity was monitored by recording the formation of NADPH spectrophotometrically at 340 nm.

Kinetics data for ASA and P_i were collected (Table 1) and found to be in reasonable agreement with literature values.[33] Inhibition data were obtained by varying the concentration of ASA and of P_i in presence of varying concentrations of inhibitor. The resulting initial velocity data were fit to the Hanes–Woolf and Lineweaver–Burk plots (ESI†).[34] The mixture of phosphonates **18a** and **18b** was found to have K_i values of 2.64 mM *vs.* ASA and 7.67 mM *vs.* inorganic phosphate. Phosphate **17b** showed K_i values comparable to the phosphonate mixture (5.78 mM *vs.* ASA and 6.49 mM *vs.* P_i), while the phosphate **17a** was around two-fold poorer as an inhibitor (13.97 mM *vs.* ASA and 11.9 mM *vs.* P_i). All three were found to inhibit in a competitive or mixed mode against ASA and in an uncompetitive mode against inorganic phosphate.

Discussion

The key finding in this study was that cyclisation of the linear inhibitor **15**[15] by a one carbon linker to generate the cyclic compounds **18a** and **18b** resulted in a change from no detectable inhibition to low millimolar inhibition. We propose that this improvement to inhibition must derive from the reduction of the entropic barrier to binding arising from the prior locking of the inhibitor conformation. The observed similarity in inhibition constants between the *cis*-phosphate **17b** and phosphonate **18** contrasts with the simulated docking results, which suggested that the extra oxygen of the phosphate should infer worse binding characteristics. It is likely, therefore, that the simulated docking did not provide an accurate simulation of real-world binding.

Some information can be ascertained from the binding modes of the respective inhibitors. Phosphates **17a** and **17b** inhibit against ASA by two different modes—compound **17a** shows non-competitive inhibition while compound **17b** shows competitive inhibition. The differences in K_i and in inhibition mode are most likely related to the different diastereomeric complimentarity of **17a** and **17b** with ASADH. Compound **18** was isolated as a mixture of diastereoisomers and the inhibition mode will therefore reflect this heterogeneity. The inhibition mode of the mixture **18** against ASA is competitive. Both diastereoisomers may be competitive inhibitors but it is more likely that the inhibition matches the diastereomeric complementarity seen with **17a** and **17b**—only one diastereoisomer is a competitive inhibitor but this dominates over the effect of the weaker inhibitor. The inhibition mode against P_i in all cases was uncompetitive, indicating that the inhibitors do not occupy the same binding site as P_i.

The results of the inhibition assay did not agree fully with the predictions of the simulated docking software. The software had predicted that phosphonate **18a** should bind better than phosphate **17a**, however, inhibition was found to be in the same range. Furthermore, the software had predicted that the phosphonate should bind in an orientation that competed with both ASA and P_i—*i.e.* binding to both regions of the active site. The *in vitro* results suggest that the phosphonate and phosphate inhibitors are only competitive with ASA and not with P_i. This may indicate that the *in vitro* binding mode of the inhibitors is different to that predicted by the software.

The software does, however, predict a previously unknown hydrogen-bonding interaction between substrate and NADPH, which could aid in the explanation of three features of ASADH catalysis. It has been noted that in the catalytic mechanism, NADPH and P_i perform roles in non-overlapping elementary steps and there is therefore no requirement for both to be bound at the same time. Kinetic evidence, however, shows that P_i remains bound throughout the oxidoreductive stage and that NADPH remains bound throughout the phosphate thiolysis stage,[14] which could be explained by favourable binding between NADPH and the phosphate group. Secondly, a hydrogen bond involving the protonated OH of the phosphate group would explain the documented advantage of ASADH inhibitors having a high pK_{a2}.[15] Thirdly, the NADPH 2′OH has been observed to locate in a similar spatial position in 1GL3 and 1YS4 when much of the rest of the NADPH molecule differs. This interaction therefore requires further real-world investigation.

Investigation of the predicted binding of the natural substrate BAP **2** suggests some interesting aspects of substrate binding. The γ-carbonyl bound relatively far away from the active site nucleophile (*ca.* 4 Å). The phosphate functional group is in the phosphate binding region of the active-site, which forces the carbonyl to adopt a position close to the phosphate binding site. The phosphate binding site is necessarily removed from the active site nucleophile to ensure that the acyl intermediate does not favour the bound phosphate too heavily over the NADPH hydride. To accompany movement of the substrate γ-carbonyl towards C135, the BAP amine group must rotate away from C135 to make full use of interaction with the Q241 residue.

Conclusions

Cyclisation of the linear inhibitor **15**[15] to the cyclic inhibitor **18** leads to an increase in inhibitory activity which we suspect can be directly attributed to the decreased entropic cost of binding. Simulated docking suggests that phosphonate **18a** should bind at both ASA and phosphate binding sites but *in vitro* results suggest a different binding mode to that predicted. A new mode of substrate–ligand binding is highlighted by the computational docking, whereby the substrate forms a hydrogen bond with the NADPH cofactor and further confirmation of this interaction must be performed. An extensive screen of reaction conditions for the synthesis of secondary carbon to phosphorus bonds was conducted, encompassing many literature reported conditions, and it was found that no conditions provided the desired material except thioketone mediated bond formation.

Experimental

Computational

PyMol (DeLano scientific)[35]. PyMOL Release 0.99 was used for all enzyme related graphics.

CORINA (Molecular networks)[36]. CORINA version 3.46 with the Corina.direct version 3.2 graphical user interface was used to generate three-dimensional structure coordinates of BAP and all putative inhibitors. When running Corina, all possible enantiomers and diastereoisomers were generated and saved in the multimol2 (.mol2) file format.

Simulated docking. The PDB coordinate file 1GL3 was used in all simulated docking experiments. Subunit A was used in all cases, and prior to docking the SMCS atom coordinates were manually removed. Proton coordinates were calculated either by using the Pymol algorithm or by using the FlexX software algorithm. Docking was performed using FlexX version 1.13.5 L implemented in Tripos Sybyl.[18] Default settings were used. The active site was defined as a 10 Å sphere centred around the Cys135 sulfur and the software was instructed to include the NADPH cofactor in the docking run. Further simulated docking was performed using the standalone FlexX version 3.1.3 (64 bit).[18] The Corina version 3.46 plugin for FlexX was used to generate ring-flip conformers for relevant ligands. The active site was set as a 10 Å sphere around the Cys135 sulfur and the software was instructed to include the NADPH cofactor in the docking run. Cys135 was set as the thiolate, and His274 as the imidazolium. No pharmacophore was set. The ligand settings were changed so that the software performed no manipulation of the protons and charges. The docking and scoring parameters were all left as the defaults. The results of the simulated docking runs were analysed in PyMol by constructing overlays of the FlexX pose coordinates.

Chemistry. All reactions were performed under a nitrogen atmosphere with dry solvent under anhydrous conditions, unless otherwise noted. Dry, deoxygenated diethyl ether (Et_2O), tetrahydrofuran (THF), acetonitrile (MeCN), toluene, dichloromethane (DCM) and hexane were obtained by passing commercially available pre-dried, oxygen-free formulations through activated alumina columns. Anhydrous ethanol was obtained by distillation from Mg/I_2. Anhydrous methanol was purchased commercially (HPLC grade). All water used was previously deionised. Yields refer to chromatographically and spectroscopically (^{1}H NMR) homogeneous materials. Reagents were purchased at the highest commercial quality and used without further purification, unless otherwise stated. Reactions were monitored by thin-layer chromatography (TLC) performed on 0.2 mm Merck silica gel glass plates (60F-254) and visualised using ultraviolet light (254 nm) and by potassium permanganate and heat as developing agents. Merck silica gel (60, particle size 0.035–0.070 mm) was used for flash column chromatography. NMR spectra were recorded on JEOL delta/GX270 (Δ270), JEOL delta/GX400 (Δ400), JEOL lamba300 (Λ300), Eclipse + 400 (E400), Varian 400 (V400) and Varian 500 (V500) instruments. NMR spectra were obtained at 298 K unless otherwise stated and samples run as a dilute solution of the stated solvent. All NMR spectra were referenced to the residual undeuterated solvent as an internal reference. The following abbreviations were used to explain the multiplicities: s = singlet, d = doublet, t = triplet, q = quartet, m = multiplet, br = broad. High resolution mass spectra (HRMS) were recorded on a magnetic sector VG Autospec using EI (electron ionisation) and CI (chemical ionisaton). High resolution mass spectra were recorded on a Bruker Apex FT–ICR–MS using ESI (electrospray ionisation). Infrared (IR) spectra were recorded on a Perkin-Elmer FT-IR Paragon 1000 spectrometer under neat conditions using a universal attenuated total reflection (UATR) attachment. Melting points were obtained on an electrothermal melting point apparatus and are uncorrected. Optical rotations were measured with a Bellingham + Stanley ADP220 polarimeter using a 1 dm optical cell. Elemental analyses were performed in the microanalytical laboratories of the University of Bristol. GC–MS (gas chromatography–mass spectrometry) data were obtained using an Agilent 6890 series gas chromatograph system with an Agilent 5973 network mass selective detector (EI mode). A 30 m × 0.25 mm, 0.25 μm film Gamma Dex column was used as the stationary phase. Injection performed with injector at 200 °C, oven temperature started and held at 70 °C for 1 min, ramped at 25 °C·min^{-1} to 150 °C, ramped at 45 °C·min^{-1} to 250 °C, held at 250 °C for 3 min, ramped at 45 °C·min^{-1} to 300 °C and held at 300 °C for 3 min. Total ion current trace was obtained for positive electron ionisation (EI+). LC–MS (high performance liquid chromatography–mass spectrometry) was performed using a Micromass Platform LC (ESI+ mode). The stationary phase was a 25 cm × 4.6 mm Phenomenex Luna 5 μ column with 5 μm C_{18} packing. The solvent system started at 75% H_2O/25% MeCN, ramped to 95% MeCN over 13 min and held for a further 2 min. All cyclic structures presented are numbered with priority given to the amino acid moiety: the α-amino carbon is consistently numbered '1'. All data for reproduction of literature syntheses can be found in the ESI†.

***N*-Cbz-5-(*R*)-dibenzylphosphate-(*S*)-*tert*-butylpipecolate, 27a.**

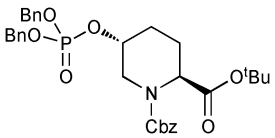

To an anhydrous 25 ml round-bottom flask, under an inert atmosphere (N_2) and with magnetic stirring, was added the *trans*-alcohol **25a** (222 mg, 0.66 mmol) and anhydrous DCM (4.4 ml). The reaction was cooled to −20 °C (external temperature) and pyridine (dist. 214 μl, 2.65 mmol) added in one portion. To this was added dibenzylphosphoryl iodide solution (0.18 M in DCM, 4.4 ml, 0.79 mmol) dropwise over 15 min. The solution turned yellow and a precipitate formed over the period of addition. The mixture was stirred at −20 °C for 30 min, then warmed to room temperature and stirred for another 2 h. The precipitate was filtered off and the filtrate reduced *in vacuo*. The resulting oil was extracted between water (6 ml) and Et_2O (25 ml). The layers were separated and the aqueous was further extracted with Et_2O (2 × 25 ml). The combined organics

were washed with $KHSO_4$ (0.3 M; 10 ml), $NaHCO_3$ (saturated; 10 ml) and brine (10 ml). The organic layer was dried ($MgSO_4$), filtered and reduced *in vacuo* to give the crude product (288 mg) as a white cloudy oil. Purification was performed by column chromatography (10% EtOAc in DCM used as eluent, R_F = 0.13) to give the target phosphate **27a** as a clear oil (234 mg, 0.393 mmol, 59.5%). $[\alpha]^{20}_D$ = −20.0 (*c* 0.07, DCM); 1 : 1 mixture of rotamers; δH (E400, 400 MHz, $CDCl_3$) 7.37–7.24 (15H, m, Ar*H*), 5.25–4.92 (6H, m, 3 × ArCH_2), 4.90–4.86 (0.5H, m, 0.5 × *H*-2_{eq}), 4.74 (0.5H, d, *J* = 4.6, 0.5 × *H*-2_{eq}), 4.66–4.61 (0.5H, m, 0.5 × *H*-5_{eq}), 4.56–4.51 (0.5H, m, 0.5 × *H*-5_{eq}), 4.34 (0.5H, d, *J* = 14.7, 0.5 × *H*-6_{eq}), 4.25 (0.5H, d, *J* = 14.7, 0.5 × *H*-6_{eq}), 3.28 (0.5H, d, *J* = 14.7, 0.5 × *H*-6_{ax}), 3.17 (0.5H, d, *J* = 14.7, 0.5 × *H*-6_{ax}), 2.09–1.83 (3H, m, 2 × *H*-4 and *H*-3_{eq}), 1.52–1.45 (1H, m, *H*-3_{ax}); 1.44 (4.5H, s, 0.5 × C(CH_3)$_3$), 1.40 (4.5H, s, 0.5 × C(CH_3)$_3$), δC (E400, 100 MHz, $CDCl_3$) 170.3 & 170.2 (ester *C*═O), 156.4 & 156.0 (carbamate *C*═O), 136.4 & 136.3 (quaternary Cbz-Ar*C*H), 135.8, (d, *J* = 6.9, 1 × quaternary phosphate-Ar*C*), 135.6, (d, *J* = 6.9, 1 × quaternary phosphate-Ar*C*), 128.5, 128.4, 128.4, 127.9, 127.9, 127.8, 127.8, 127.8, 127.7, 81.9 & 81.8 (*C*(CH$_3$)$_3$), 70.9 (d, *J* = 5.4, 0.5 × C^5), 70.8 (d, *J* = 5.4, 0.5 × C^5), 69.2–69.1 (m, 2 × ArCH_2P), 67.3 & 67.2 (Cbz-ArCH_2), 54.3 & 53.9 (C^2), 45.9 (d, *J* = 5.4, 0.5 × C^6), 45.8 (d, *J* = 5.4, 0.5 × C^6), 27.9 & 27.9 (C(*C*H$_3$)$_3$), 25.8 (d, *J* = 3.8, 0.5 × C^4), 25.6 (d, *J* = 3.8, 0.5 × C^4), 20.3 & 20.1 (C^3); δP (E400, 162 MHz, $CDCl_3$) −0.88, −1.01; ν_{max} (neat) cm^{-1} 3034 (ArC–H), 2976 (C–H), 1731 (ester C═O), 1702 (carbamate C═O); ESIMS *m*/*z* 634 ([M]K^+ 3%), 618 ([M]Na^+ 100%), 596 (16%), 206 (6%); HRMS ESI calcd. for $C_{32}H_{38}NO_8PNa$ ([M]Na^+) 618.2227, found 618.2230; anal. calcd. (%) for $C_{32}H_{38}NO_8P$ C 64.53, H 6.43, N 2.35, found C 64.23, H 6.68, N 2.52.

***N*-Cbz-5-(*S*)-dibenzylphosphate-(*S*)-*tert*-butylpipecolate, 27b.**

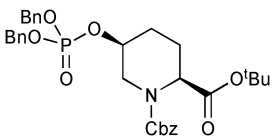

To an anhydrous 25 ml round-bottom flask, under an inert atmosphere (N_2) and with magnetic stirring, was added the *cis*-alcohol **25b** (405 mg, 1.20 mmol) and anhydrous DCM (8 ml). The reaction was cooled to −20 °C (external temperature) and pyridine (dist. 387 µl, 4.80 mmol) added in one portion. To this was added dibenzylphosphoryl iodide solution (0.18 M in DCM, 8 ml, 1.44 mmol) dropwise over 15 min. The solution turned yellow and a precipitate formed over the period of addition. The mixture was stirred at −20 °C for 30 min, then warmed to room temperature and stirred for another 2 h. The precipitate was filtered off and the filtrate reduced *in vacuo*. The resulting oil was extracted between water (7 ml) and Et_2O (27 ml). The layers were separated and the aqueous was further extracted with Et_2O (2 × 27 ml). The combined organics were washed with $KHSO_4$ (0.3 M; 10 ml), $NaHCO_3$ (saturated; 10 ml) and brine (10 ml). The organic layer was dried ($MgSO_4$), filtered and reduced *in vacuo* to give the crude product (543 mg) as a white cloudy oil. Purification was performed by column chromatography (15% EtOAc in $CHCl_3$ used as eluent, R_F = 0.30) to give the target phosphate **27b** as a clear oil (466 mg, 0.783 mmol, 65.3%). $[\alpha]^{23}_D$ = −15.0 (*c* 0.01, DCM); 1 : 1 mixture of rotamers; δH (V400, 400 MHz, $CDCl_3$) 7.40–7.28 (15H, m, Ar*H*), 5.25–4.99 (6H, m, 3 × ArCH_2), 4.76 (0.5H, d, *J* = 4.5, 0.5 × *H*-2_{eq}), 4.63 (0.5H, d, *J* = 4.7, 0.5 × *H*-2_{eq}), 4.37 (0.5H, dd, *J* = 12.7, 5.3, 0.5 × *H*-6_{eq}), 4.29–4.16 (1.5H, m, 0.5 × *H*-6_{eq} and *H*-5_{ax}), 2.95 (0.5H, dd, *J* = 12.7, 10.6, 0.5 × *H*-6_{ax}), 2.85 (0.5H, dd, *J* = 11.2, 10.6, 0.5 × *H*-6_{ax}), 2.29–2.19 (1H, m, *H*-4_{eq}), 2.10–1.99 (1H, m, *H*-3_{eq}), 1.68–1.57 (1H, m, *H*-4_{ax}); 1.45 (4.5H, s, 0.5 × C(CH_3)$_3$), 1.42 (4.5H, s, 0.5 × C(CH_3)$_3$), 1.41–1.30 (1H, m, *H*-3_{ax}), δC (E400, 100 MHz, $CDCl_3$) 169.6 & 169.5 (ester *C*═O), 155.8 & 155.6 (carbamate *C*═O), 136.4 & 136.4 (quaternary Ar*C*), 135.8–135.8 (m, 2 × quaternary phosphate-Ar*C*), 128.5, 128.4, 128.0, 127.9, 127.8, 127.8, 82.1 & 82.0 (*C*(CH$_3$)$_3$), 72.5 (d, *J* = 5.0, 0.5 × C^5), 72.4 (d, *J* = 5.0, 0.5 × C^5), 69.4–69.2 (m, 2 × ArCH_2P), 67.5 & 67.4 (2 × Cbz-ArCH_2), 53.8 & 53.5 (C^2), 45.9 (d, *J* = 4.0, 0.5 × C^6), 45.8 (d, *J* = 5.0, 0.5 × C^6), 28.3 & 28.3 (C^3), 27.9 & 27.8 (C(*C*H$_3$)$_3$), 24.6 & 24.5 (C^4); δP (E400, 162 MHz, $CDCl_3$) −1.1, −1.2; ν_{max} (neat) cm^{-1} 3035 (ArC–H), 2976 (C–H), 1731 (ester C═O), 1706 (carbamate C═O); ESIMS *m*/*z* 634 ([M]K^+ 19%), 618 ([M]Na^+ 100%), 540 (6%), 358 (8%), 206 (6%); HRMS ESI calcd. for $C_{32}H_{38}NO_8PNa$ ([M]Na^+) 618.2227, found 618.2257; anal. calcd. (%) for $C_{32}H_{38}NO_8P$ C 64.53, H 6.43, N 2.35, found C 64.78, H 6.60, N 2.64.

***N*-Cbz-5-(*R*)-dibenzylphosphate-(*S*)-pipecolic acid.**

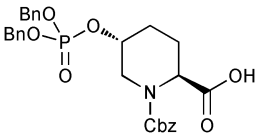

To a 25 ml round-bottom flask with magnetic stirring was added the protected phosphate **27a** (219 mg, 0.368 mmol) followed by DCM (2 ml) and TFA (2 ml). Stirring was continued until the reaction was complete by TLC (2 h). The reaction mixture was evaporated from DCM four times to remove excess TFA and then subjected to a base–acid cycle: the resulting oil was dissolved in $NaHCO_3$ (2.5%, 10.8 ml, 3.24 mmol) and extracted with Et_2O (2 × 20 ml). The aqueous was acidified to pH 1 with HCl (2 N) and extracted with EtOAc (3 × 20 ml). The acid extract organics were combined, dried ($MgSO_4$), filtered and reduced *in vacuo* to give the target material as a white foam (166 mg, 0.309 mmol, 84%) which was used without further purification. δH (V400, 400 MHz, $CDCl_3$) 8.90–8.09 (3H, br s, exchangeable O*H* & NH_2), 7.26–7.07 (15H, m, Ar*H*), 5.07–4.75 (6H, m, 3 × ArCH_2 & *H*-2_{eq}), 4.58–4.11 (2H, m, *H*-6_{eq} & *H*-5_{ax}), 3.17–3.01 (1H, m, 0.5 × *H*-5_{ax}), 2.08–1.73 (1H, m, *H*-3_{eq} & *H*-4_{eq} & *H*-3_{ax}), 1.48–1.34 (1H, m, *H*-4_{ax}).

***N*-Cbz-5-(*S*)-dibenzylphosphate-(*S*)-pipecolic acid.**

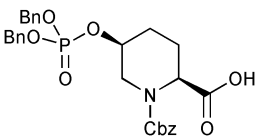

To a 25 ml round-bottom flask with magnetic stirring was added the protected phosphate **27b** (644 mg, 1.08 mmol) followed by DCM (4 ml) and TFA (4 ml). Stirring was

continued until the reaction was complete by TLC (2 h). The reaction mixture was evaporated from DCM four times to remove excess TFA and then subjected to a base–acid cycle: the resulting oil was dissolved in $NaHCO_3$ (2.5%, 10.8 ml, 3.24 mmol) and extracted with Et_2O (2 × 20 ml). The aqueous was acidified to pH 1 with HCl (2 N) and extracted with EtOAc (3 × 20 ml). The acid extract organics were combined, dried ($MgSO_4$), filtered and reduced *in vacuo* to give the target material as a white foam (346.9 mg, 0.646 mmol, 60%) which was used without further purification. δH (V400, 400 MHz, $CDCl_3$) 9.18–8.95 (3H, br s, exchangeable O*H* & NH_2), 7.38–7.20 (15H, m, Ar*H*), 5.15–4.71 (6H, m, 3 × ArCH_2 & *H*-2_{eq}), 4.43–4.08 (2H, m, *H*-6_{eq} & *H*-5_{ax}), 3.03–2.84 (1H, m, 0.5 × *H*-5_{ax}), 2.32–2.18 (1H, m, *H*-3_{eq}), 2.16–2.98 (1H, m, *H*-4_{eq}), 1.71–1.56 (3H, m, *H*-3_{ax}), 1.51–1.35 (1H, m, *H*-4_{ax}).

Pipecolic acid-5-(*R*)-phosphate hydrochloric acid salt, 17a.

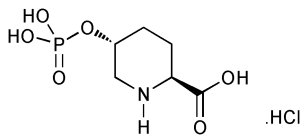

To a 25 ml round-bottom flask, under an inert atmosphere (N_2) and with magnetic stirring, was added the *N*-Cbz-5-(*S*)-dibenzylphosphate-(*S*)-pipecolic acid (166 mg, 0.309 mmol). This was dissolved in EtOH (10 ml) and Pd/C (10% 20 mg) added. The reaction was stirred under a hydrogen atmosphere for 20 h. The suspension was filtered through celite and washed with water (25 ml). The resulting solution was acidified with HCl (2 N, 5 ml) and freeze-dried to provide the target salt **17a** (46 mg, 0.15 mmol, 49%) as a yellow hygroscopic solid. $[\alpha]^{23}{}_D$ = −10.00 (*c* 0.008, H_2O); δH (V400, 400 MHz, D_2O) 4.36–4.27 (1H, m, *H*-5_{ax}), 4.02 (1H, dd, *J* = 7.3, 4.4, *H*-2_{ax}), 3.39 (1H, dd, *J* = 12.7, 3.2, *H*-6_{eq}), 3.12 (1H, dd, *J* = 12.7, 7.1, *H*-6_{ax}), 2.27–2.16 (1H, m, *H*-3_{eq}); 1.92–1.80 (2H, m, *H*-3_{ax} and *H*-3_{eq}); 1.77–1.65 (1H, m, *H*-4_{eq}); δC (V400, 100 MHz, D_2O) 170.4 (carbonyl), 67.2 (d, *J* = 4.7, C^5), 54.7 (C^2), 45.6 (d, *J* = 5.5, C^6), 26.6 (d, *J* = 3.9, C^4), 21.0 (C^3); δP (V400, 162 MHz, D_2O) −1.2; ν_{max} (neat) cm^{-1} 3600–2400 (br s, acid O–H and ammonium N–H), 1726 (acid C|O); ESIMS (negative ion mode) *m*/*z* 449 ([2M–H]$^-$ 5%), 224 ([M–H]$^-$ 100%); HRMS ESI (negative ion mode) calcd. for $C_6H_{11}NO_6P$ ([M–H]$^-$) 224.0329, found 224.0329.

Pipecolic acid-5-(*S*)-phosphate hydrochloric acid salt, 17b.

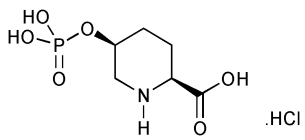

To a 25 ml round-bottom flask, under an inert atmosphere (N_2) and with magnetic stirring, was added *N*-Cbz-5-(*R*)-dibenzylphosphate-(*S*)-pipecolic acid (346.9 mg, 0.646 mmol). EtOH (15 ml) and Pd/C (10% 20 mg) were added. The reaction was stirred under a hydrogen atmosphere for 20 h. The suspension was filtered through celite and washed with water (25 ml). The resulting solution was acidified with HCl (2 N, 5 ml) and freeze-dried to provide the target salt **17b** (151 mg, 0.49 mmol, 76%) as a yellow hygroscopic solid. $[\alpha]^{23}{}_D$ = −8.40 (*c* 0.08, H_2O); δH (V400, 400 MHz, D_2O) 4.47 (1H, dm, *J* = 8.6, *H*-5_{eq}), 3.86 (1H, dd, *J* = 12.5, 3.4, *H*-2_{ax}), 3.39 (1H, dm, *J* = 13.7, *H*-6_{eq}), 3.12 (1H, dm, *J* = 13.7, *H*-6_{ax}), 2.09–1.82 (3H, m, *H*-*4* and *H*-3_{eq}), 1.75–1.65 (1H, m, *H*-3_{ax}); δC (V400, 100 MHz, D_2O) 170.5 (carbonyl), 66.7 (d, *J* = 5.5, C^5), 56.1 (C^2), 47.7 (d, *J* = 5.5, C^6), 27.0 (d, *J* = 3.1, C^4), 19.8 (C^3); δP (V400, 162 MHz, D_2O) −1.4; ν_{max} (neat) cm^{-1} 3600–2400 (br s, acid O–H and ammonium N–H), 1728 (acid C|O); ESIMS (negative ion mode) 449 ([2M–H]$^-$ 26%), 224 ([M–H]$^-$ 100%); HRMS ESI (negative ion mode) calcd. for $C_6H_{11}NO_6P$ ([M–H]$^-$) 224.0329, found 224.0338.

***N*-Cbz-5,6-dehydro-5-thiol-*tert*-butyl-(*S*)-pipecolate, 28.**

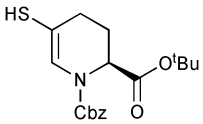

To a boiling-tube, under an inert atmosphere (N_2) and with magnetic stirring, was added the 5-keto pipecolate **23** (3.33 g, 10 mmol), DMF (2 ml) and morpholine (86 µl, 1 mmol). The reaction mixture was equipped with a $CO_{2(s)}$/acetone condenser. The reaction vessel was charged with H_2S gas, which was trapped by the condenser and allowed to drip back into the reaction mixture. The reaction vessel was held in an oil bath that was maintained at 10 °C. The reaction vessel was recharged with H_2S every 1 h for a total of 5 h. The reaction mixture was then quenched by pouring onto ice and acidifying with 2 N HCl until acidity persisted. The acidified aqueous layer was extracted with EtOAc (3 × 50 ml), and this organic layer was further washed with water until the water extracts were of neutral pH. The organic layer was dried ($MgSO_4$), filtered and reduced *in vacuo* to give a yellow oil (3.71 g). Purification was performed by chromatography (15% EtOAc in hexane, R_F of enethiol **28** = 0.25, R_F of trimer **29** = 0.14) to give recovered starting material in 20% yield and the enethiol **28** as a pale yellow solid (209 mg, 0.60 mmol, 6%). $[\alpha]^{23}{}_D$ = −45.4 (*c* 0.09, DCM); mp = 70–74 °C (neat); 1 : 1 mixture of rotamers; δH (Λ300, 300 MHz, $CDCl_3$) 7.41–7.32 (5H, m, Ar*H*), 7.22 & 7.11 (1H, s, C*H*-*6*), 5.27 & 5.12 (1H, d, *J* = 12.3, 0.5 × ArCH_2), 5.25 & 5.19 (1H, d, *J* = 12.1, 0.5 × ArCH_2), 4.82–4.78 & 4.71–4.67 (1H, m, *H*-*2*), 2.57 & 2.54 (1H, q, *J* = 0.9, S*H*), 2.42–1.87 (4H, m, *H*-*3* & *H*-*4*), 1.45 & 1.38 (9H, s, C(CH_3)$_3$), δC (V400, 100 MHz, $CDCl_3$) 169.5 & 169.3 (ester *C*|O), 152.8 & 152.7 (carbamate *C*|O), 135.8 (quaternary Cbz-Ar*C*H), 128.6, 128.5, 128.3, 128.2, 128.0, 125.9 & 125.8 (C^6), 104.5 & 103.9 (C^5), 82.0 & 81.9 (*C*(CH$_3$)$_3$), 68.1 & 67.8 (Cbz-ArCH$_2$), 53.6 & 53.2 (C^2), 28.2 & 27.8 (C^3), 27.9 & 27.8 (C(*C*H$_3$)$_3$), 24.3 & 24.1 (C^4), ν_{max} (neat) cm^{-1} 3105 alkene C–H, 3037 (Ar C–H), 2979 (C–H), 2945 (C–H), 2889 (C–H), 2843 (C–H), 2544 (S–H), 1736 (ester C|O), 1706 (carbamate C|O); EIMS *m*/*z* 349 ([M]$^+$ 13%), 249 ([M–$CO_2{}^tBu$ + H]$^+$ 16%), 204 (30%), 158 (12%), 91 ([Bn]$^+$ 100%); HRMS EI calcd. for $C_{18}H_{23}NO_4S$ ([M]$^+$) 349.1348, found 349.1352. anal. calcd. (%) for $C_{18}H_{23}NO_4S_3$ C 61.87, H 6.63, N 4.01, S 9.18, found C 61.68, H 6.60, N 4.00, S 9.42.

_N_-Cbz-5-thioketone-(_S_)-_tert_-butylpipecolate trimer, 29.

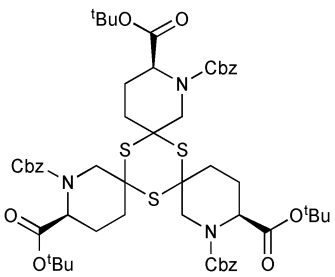

The trimer **29** was obtained as a highly deliquescent white foam (1.72 g, 1.64 mmol, 49%). $[\alpha]^{24}_D$ = +11.3 (_c_ 0.5, DCM); δH (Λ300, 300 MHz, $CDCl_3$) 7.44–7.26 (5H, m, Ar*H*), 5.30–5.06 (2H, m, ArCH_2), 4.97–4.57 (1H, m, *H-2*), 4.34–4.08 (1H, m, *H-6*$_{eq}$), 3.43–3.17 (1H, m, *H-6*$_{ax}$), 2.55–1.56 (4H, m, *H-3* & *H-4*), 1.51–1.31 (9H, m comprising at least 10 singlets, C(CH_3)$_3$); ν_{max} (neat) cm^{-1} 3067 (ArC–H), 3034 (ArC–H), 2977 (C–H), 2934 (C–H), 1704 (C|O); EIMS *m*/*z* 349 ([thione]$^+$ 15%), 249 ([M–$CO_2{}^t$Bu]$^+$ 29%), 204 (52%), 158 ([M–^{t}Bu–Cbz + H]$^+$ 21%), 91 ([Bn]$^+$ 100%); anal. calcd. (%) for $C_{54}H_{69}N_3O_{24}P_3S_3$ C 61.87, H 6.63, N 4.01, S 9.18, found C 62.00, H 6.81, N 4.01, S 9.06.

_N_-Cbz-5-dimethylphosphonate-5-methylthioether-(_S_)-_tert_-butylpipecolate, _trans_ (30a) and _cis_ (30b) isomer mixture.

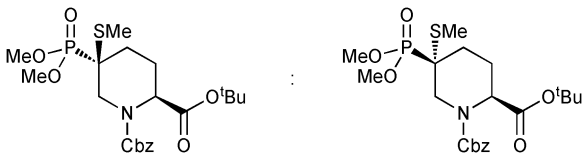

To an anhydrous 25 ml round-bottom flask, under an inert atmosphere (N_2) and with magnetic stirring, was added the trimer **29** (1.0 g, 2.86 mmol). This was followed by anhydrous toluene (10 ml) and P(OMe)$_3$ (1.23 ml, 10.4 mmol). The reaction was heated under reflux until no starting material could be detected by GC–MS (40 h), cooled to room temperature and solvent reduced by blowing with N_2. Purified by column chromatography (15% EtOAc in hexane, R_F of thioether **30a** and **30b** = 0.24) gave the target material as a clear oil (899 mg, 1.90 mmol, 67%). Obtained as a 2 : 1 mixture of the *trans* : *cis* isomers: $[\alpha]^{24}_D$ = −22.03 (_c_ 0.3, DCM); δH (E400, 400 MHz, d_6-DMSO) 7.42–7.28 (5H, m, Ar*H*), 5.23–5.01 (2H, m, Cbz-ArCH_2), 4.79–4.71 (0.67H, *trans-H-2*$_{eq}$), 4.57–4.51 (0.33H, *cis-H-2*$_{eq}$), 4.49–4.30 & 3.24–3.10 (0.67H, m, *cis*-H-6$_{eq+ax}$), 4.04–3.96 & 3.49–3.32 (1.33H, m, *trans*-H-6$_{eq+ax}$), 3.78–3.57 (6H, m, P(OCH_3)$_2$), 2.23 & 2.21 (1H, *cis*-SCH_3), 2.13 & 2.08 (2H, *trans*-SCH_3), 2.25–1.71 (4H, m, *H-3* & *H-4*), 1.41 & 1.37 (6H, C(CH_3)$_3$), 1.40 & 1.36 (3H, C(CH_3)$_3$); δC (E400, 100 MHz, d_6-DMSO) 170.2 & 170.1 (ester *C*|O), 155.9 & 155.1 (carbamate *C*|O), 137.1 & 137.0 (quaternary Cbz-ArCH), 129.0, 128.9, 128.6, 128.5, 128.4, 128.2, 128.0, 127.9, 82.3 & 79.7 (*C*(CH$_3$)$_3$), 67.4 & 67.2 & 67.2 & 67.2 (Cbz-ArCH_2), 54.8, 54.6, 54.5, 54.5, 54.4, 54.4, 54.2, 54.0, 53.9, 53.9, 45.3 (*cis-C*^{6}), 45.7 (*trans-C*^{6}), 28.1, 28.0, 23.9, 23.9, 22.7 & 22.7 (C(CH_3)$_3$); δP (Λ300, 122 MHz, $CDCl_3$) 28.8 & 28.7 (0.4P), 26.2 & 25.9 (0.6P); ν_{max} (neat) cm^{-1} 3010 (Ar C–H), 2942 (C–H), 1731 (ester C|O), 1702 (carbamate C|O), 1244 (P|O); S–H absorption absent; CIMS *m*/*z* 474 ([M]H$^+$ 7%), 418 ([M–^{t}Bu + H]H$^+$ 88%), 374 ([M–$CO_2{}^t$Bu + H]H$^+$ 53%), 372 ([M–$CO_2{}^t$Bu]$^+$ 55%), 360 (23%), 328 (44%), 236 (21%), 91 ([Bn]$^+$ 100%), (thiol [M]H$^+$ = 460; not observed); HRMS CI calcd. for $C_{21}H_{33}NO_7SP$ ([M]H$^+$) 474.1715, found 474.1715.

_N_-Cbz-5-dimethylphosphonate-(_S_)-_tert_-butylpipecolate, _trans_ (32a) and _cis_ (32b) isomer mixture.

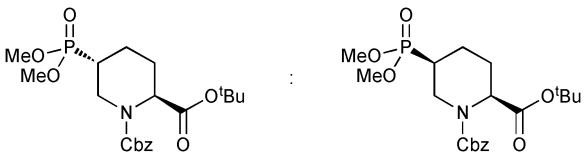

To an anhydrous 50 ml round-bottom flask, under an inert atmosphere (N_2) and with magnetic stirring was added the 2 : 1 mixture of α-thioether phosphonates **30a** and **30b** (489 mg, 1.03 mmol) followed by EtOH (anh; 15 ml). Raney nickel (10 g, 50% slurry in H_2O) was washed with EtOH (anh; 3 × 5 ml) and added to the reaction mixture. The reaction mixture was stirred until complete by TLC (2 h) and filtered through celite. The solvent was removed *in vacuo* and re-suspended in DCM (5 ml). The reaction vessel was cooled in an ice-bath and then DIPEA (400 µl, 2.30 mmol) and Cbz-Cl (150 µl, 1.05 mmol) added. The reaction mixture was allowed to warm to room temperature over 20 min and then extracted between HCl (0.5 N, 2 0 ml) and EtOAc (3 × 25 ml). The combined organics were dried ($MgSO_4$), filtered and reduced *in vacuo* to give a yellow oil (280 mg). Purification was performed by column chromatography (20% EtOAc in hexane, R_F = 0.26) gave the target material as a clear oil (349 mg, 0.82 mmol, 79%). Obtained as a 2 : 1 mixture of the *trans* : *cis* isomers and 1 : 1 mixture of rotamers: δH (E400, 400 MHz, $CDCl_3$) 7.43–7.41 (5H, m, Ar*H*), 5.27–5.07 (2H, m, ArCH_2), 4.88 (0.17H, d, *J* = 5.9, *H-2*), 4.81–4.66 (0.67H, m, *H-2*), 4.75 (0.17H, d, *J* = 5.9, *H-2*), 4.38–4.21 (1H, m, *H-6*$_{eq}$), 3.80–3.61 (6H, m, P(O)(OCH_3)$_2$), 3.59–3.47 (0.33H, m, *H-6*$_{ax}$), 3.48–3.39 (0.33H, m, *H-6*$_{ax}$), 3.19 (0.17H, ddd (dd ^{31}P decoupled), *J* = 12.9, 12.1, 3.9, *H-6*$_{ax}$), 3.07 (0.17H, ddd (dd ^{31}P decoupled), *J* = 12.6, 11.9, 3.9, *H-6*$_{ax}$), 3.98–1.69 (5H, m, *H-5* & *H-3*$_{eq}$ & *H-3*$_{ax}$ & *H-4*$_{eq}$ & *H-4*$_{ax}$), 1.49–1.42 (9H, C(CH_3)$_3$), δC (Λ300, 76 MHz, $CDCl_3$) 170.2 & 169.7 & 169.6 (ester *C*|O), 155.8 & 155.6 & 155.5 & 155.5 (carbamate *C*|O), 136.3 & 136.3 & 136.2 (quaternary Ar*C*), 128.3, 128.2, 128.2, 127.8, 127.7, 127.7, 127.6, 81.8 & 81.7 & 81.4 (*C*(CH$_3$)$_3$), 67.1 & 67.1 & 67.0 (ArCH_2), 54.3 & 54.2 & 53.9 (*C*^{2}), 62.4 & 52.3 & 52.2 & 52.1 (P(O)(OCH_3)$_2$), 39.6–39.2 (m, *C*^{6}), 34.5, 34.3, 32.6, 32.4, 31.2, 31.2, 30.1, 29.3, 28.6, 27.7 & 27.7 (C(*C*H$_3$)$_3$), 27.5, 26.2, 26.0, 22.8, 22.8, 20.7, 20.6, 20.3, 20.3. δP (Λ300, 122 MHz, $CDCl_3$) 33.8, 31.3; ν_{max} (neat) cm^{-1} 2954 (C–H), 2869 (C–H), 1731 (ester), 1702 (carbamate); CIMS *m*/*z* 428 ([M]H$^+$ 14%), 372 ([M–^{t}Bu + H]H$^+$ 55%), 328 (100%), 326 ([M–$CO_2{}^t$Bu]$^+$ 38%), 282 (67%), 192 (23%), 91 ([Bn]$^+$ 100%); HRMS CI calcd. for $C_{20}H_{31}NO_7P$ ([M]H$^+$) 428.1838, found 428.1841; anal. calcd. (%) for $C_{20}H_{30}NO_7P$ C 56.20, H 7.07, N 3.28, found C 56.247, H 7.327, N 3.456.

_N_-Cbz-5-dimethylphosphonate-(_S_)-pipecolic acid, _cis_ and _trans_ isomer mixture.

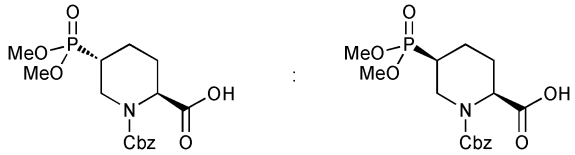

To a 25 ml round-bottom flask, under an inert atmosphere (N_2) and with magnetic stirring was added the 2 : 1 mixture of phosphonates **32a** and **32b** (398 mg, 0.93 mmol) followed by DCM (3 ml) and TFA (3 ml). The reaction mixture was stirred until complete by TLC (2 h) and the solvent removed *in vacuo*. The resulting oil was evaporated from DCM (5 × 10 ml) to remove residual TFA, giving a brown oil (416 mg). This was extracted between $NaHCO_3$ (2.5%, 10 ml) and Et_2O (3 × 10 ml). The aqueous was then acidified using 2 N HCl until acidity persisted, at which point a white precipitate formed. Extraction with EtOAc (3 × 10 ml) removed the precipitate. The combined EtOAc layers were dried ($MgSO_4$), filtered and reduced *in vacuo* to give the deprotected acid as a clear oil (332 mg, 0.89 mmol, 96%). Obtained as a 2 : 1 mixture of the *trans* : *cis* isomers and 1 : 1 mixture of rotamers: δH (V400, 400 MHz, $CDCl_3$) 8.95–8.70 (1H, br s, OH), 7.45–7.22 (5H, m, Ar*H*), 5.29–5.07 (2H, m, ArCH_2), 5.04–5.77 (1H, m, *H-2*), 4.38–4.23 (1H, m, *H-6*$_{eq}$), 3.80–3.59 (6H, m, P(O)(OCH_3)$_2$), 3.52 (0.33H, dd, J = 14.2, 4.5, *H-6*$_{ax}$), 3.43 (0.33H, dd, J = 14.2, 4.5, *H-6*$_{ax}$), 3.23 (0.17H, ddd, J = 13.1, 12.6, 4.4, *H-6*$_{ax}$), 3.15 (0.17H, ddd, J = 13.1, 13.1, 3.9, *H-6*$_{ax}$), 2.44–1.52 (5H, m, *H-5* & *H-3*$_{eq}$ & *H-3*$_{ax}$ & *H-4*$_{eq}$ & *H-4*$_{ax}$), δC (Λ300, 76 MHz, $CDCl_3$) 174.4 & 173.4 & 173.2 (ester *C*═O), 159.0 & 158.6 & 156.2 & 155.7 (carbamate *C*═O), 136.2 & 136.2 (quaternary Ar*C*), 128.6, 128.5, 128.4, 128.0, 128.0, 127.9, 127.8, 127.8, 67.7 & 67.7 (Ar*C*H$_2$), 54.3 & 54.2 & 53.9 (*C*^{2}), 53.8, 53.5, .53.3, 53.3, 53.2, 53.1, 53.1, 53.0, 40.7, 40.7, 40.4, 40.4, 39.7, 39.4, 34.3, 34.0, 32.8, 32.6, 30.9, 29.5, 26.3, 26.1, 26.0, 22.8, 20.7, 20.6, 20.4, 20.3, 19.8. δP (Λ300, 122 MHz, $CDCl_3$) 33.9 (*trans*-P), 22.4 & 32.0 (*cis*-P); ν_{max} (neat) cm^{-1} 3750–2100 (br s, acid O–H), 2956 (C–H), 1680 (br, ester & carbamate C═O); CIMS m/z 372 ([M]H$^+$ 8%), 328 ([M–CO_2 + H]H$^+$ 54%), 282 (24%), 192 (30%), 91 ([Bn]$^+$ 100%); HRMS CI calcd. for $C_{16}H_{23}NO_7P$ ([M]H$^+$) 372.1212, found 372.1210.

5-Dimethylphosphonate pipecolic acid, _cis_ and _trans_ isomer mixture.

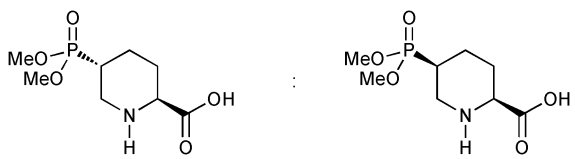

To a 25 ml round-bottom flask, under an inert atmosphere (N_2) and with magnetic stirring, was added the Cbz protected pipecolic acid 2 : 1 mixture of *cis* and *trans* *N*-Cbz-5-dimethylphosphonate-(*S*)-pipecolic acid isomers (225 mg, 0.606 mmol) followed by EtOH (15 ml). 10% Pd/C (50 mg) was added and the reaction mixture flushed with H_2 and the H_2 atmosphere maintained by balloon. The reaction was allowed to stir until complete by LCMS (20 h) and then worked up by filtration through celite. The solvent was removed *in vacuo* to yield the target material as a clear oil (102 mg, 0.433 mmol, 71%). Used in the next step without further purification. δH (Λ300, 300 MHz, $CDCl_3$) 10.22–8.07 (2H, br s, N*H* & O*H*; removed by D_2O shake), 3.77 & 3.74 (6H, s, P(OCH_3)$_2$), 3.73–2.83 (3H, m, 2 × *H-6* and *H-2*), 2.48–1.40 (5H, m, 2 × *H-3* and 2 × *H-4*); δP (Λ300, 122 MHz, $CDCl_3$) 29.9 & 29.8.

5-Phosphonic acid pipecolic acid hydrochloride salt, _trans_ (18a) and _cis_ (18b) isomer mixture.

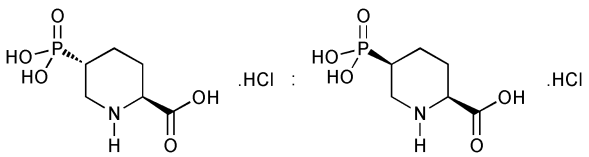

To a 50 ml round-bottom flask with magnetic stirring was added the *cis* and *trans* 5-dimethylphosphonate pipecolic acid isomeric mixture (138 mg, 0.582 mmol) followed by HCl (6 N, 10 ml). The reaction was heated to reflux and continued until complete by LCMS (5 h). The solvent was removed by blowing with N_2 to give the diastereoisomeric mixture **18a** and **18b** as a brown hygroscopic solid (HCl salt; 106 mg, 0.366 mmol, 63%). Obtained as a 2 : 1 mixture of the *trans* : *cis* isomers, integration is with respect to each isomer: δH (V400, 400 MHz, D_2O) 4.24–4.20 (1H, m, *cis H-2*), 3.83 (1H, dd, J = 12.47, *trans*, *cis H-2*), 3.51 (1H, dm, J = 1.45, *trans H-6*$_{eq}$), 3.39–3.31 (1H, m, *cis H-6*$_{eq}$), 3.21 (1H, ddd (dd, P decoupled), J = 12.96, 11.25, 6.11, *cis H-6*$_{ax}$), 2.91 (1H, ddd (dd, P decoupled), J = 13.20, 13.20, 4.65, *trans H-6*$_{ax}$), 2.31–2.24 (1H, m, *trans H-3*$_{eq}$), 2.28–2.15 (1H, m, *cis H-3*$_{eq}$), 2.13–1.98 (1H, m, *cis H-5*), 2.08–1.98 (1H, m, *trans H-4*$_{eq}$), 2.06–1.93 (1H, m, *trans H-5*), 1.92–1.82 (1H, m, *cis H-3*$_{eq}$), 1.91–1.80 (1H, m, *cis H-3*$_{ax}$), 1.68–1.53 (1H, m, *trans H-3*$_{ax}$), 1.62–1.51 (1H, m, *trans H-4*$_{ax}$), 1.51–1.39 (1H, m, *cis H-4*$_{ax}$); δC (V400, 100 MHz, D_2O) 171.3 (*cis* acid *C*═O), 170.4 (*trans* acid *C*═O), 56.2 (*trans C*^{2}), 54.1 (*cis R*^{2}), 43.9 (*trans C*^{6}), 41.3 (*cis C*^{6}), 32.5 (*cis C*^{5}), 32.0 (*trans C*^{5}), 25.1 (*trans C*^{3}), 23.3 (*cis C*^{3}), 22.6 (*trans C*^{4}), 19.5 (*cis C*^{4}); δP (V400, 162 MHz, $CDCl_3$) 22.5 (*cis*), 22.0 (*trans*); ν_{max} (neat) cm^{-1} 3600–2400 (br s, acid O–H and ammonium N–H), 1730 (acid C═O); ESIMS (negative ion mode) m/z 417 ([2M–H]$^-$ 22%), 208 ([M–H]$^-$ 100%); HRMS ESI (negative ion mode) calcd. for $C_6H_{11}NO_5P$ ([M–H]$^-$) 208.0380, found 208.0388.

Enzyme assays. Enzyme assays: stock solutions were made with deionised water and using ACS grade reagents. ASADH (homodimer; subunit M_W = 39 kDa)[12] was expressed and purified from recombinant *E. coli* (the same stock and purity used in previous publications[15,16]—provided by Dr A. Hadfield,[12] University of Bristol). The increase in NADPH concentration was observed at 340 nm over 100 seconds using a PharmaciaLKB Ultrospec III spectrophotometer equipped with a water-heated (37 °C) cuvette holder. The buffer solutions were prewarmed to 37 °C before use by immersion in a water bath. All other stock solutions were stored on ice. Assays were conducted in a far UV quartz cuvette that was fully transparent to 340 nm light.

The assay was performed in the following way (all concentrations refer to final cuvette concentration): buffer solution (bicine buffer; 900 µl, 0.2 M, pH 8.6) was introduced

into a 1000 μl quartz cuvette. The remaining assay components were then added to make up the final 100 μl. The order of addition used for K_M and K_i determination was ASADH (0.56 $\mu g \cdot ml^{-1}$), phosphate (15 mM), inhibitor (0, 0.5, 1, 2 and 5 mM) and $NADP^+$ (150 μM). ASA (50, 100, 200, 1000 and 2500 μM) was added last to start the reaction. The specific activity recorded for the production of NADPH by ASADH was 73.74 $\mu mol\ min^{-1}\ mg^{-1}$ at 1240 μM ASA, 15 mM P_i and 150 μM $NADP^+$. The cuvette was inverted twice, placed in the spectrophotometer and the subsequent reaction was monitored at 340 nm. The spectrophotometer was set up to record the absorption at 340 nm every 2s. K_M, V_{max} and K_i, were obtained from Hanes–Woolf plots (see ESI†).[34]

Referencesand notes

1 R. E. Viola, *Acc. Chem. Res.*, 2001, **34**, 339–349.
2 C. R. Faehnle, J. Le Coq, X. Liu and R. E. Viola, *J. Biol. Chem.*, 2006, **281**, 31031–31040.
3 K. Kumarasamy, *et al.*, *Lancet Infect. Dis.*, 2010, **3099**, 1–6.
4 H. Loessner, A. Endmann, M. Rohde, R. Curtiss and S. Weiss, *FEMS Microbiol. Lett.*, 2006, **265**, 81–88.
5 R. J. Cox, *Nat. Prod. Rep.*, 1996, **13**, 29–43.
6 G. A. Cardineau and R. Curtiss, *J. Biol. Chem.*, 1987, **262**, 3344–3353.
7 J. E. Galán, K. Nakayama and R. Curtiss, *Gene*, 1990, **94**, 29–35.
8 O. S. Harb and Y. Abu Kwaik, *Infect. Immun.*, 1998, **66**, 1898–1903.
9 S. Black and N. Wright, *J. Biol. Chem.*, 1955, **213**, 39–50.
10 J. Biellmann, P. Eid, C. Hirth and H. Jörnvall, *Eur. J. Biochem.*, 1980, **104**, 53–58.
11 J. Blanco, R. Moore and R. Viola, *Proc. Natl. Acad. Sci. U. S. A.*, 2003, **100**, 12613–12617.
12 A. Hadfield, G. Kryger, J. Ouyang, G. A. Petsko, D. Ringe and R. E. Viola, *J. Mol. Biol.*, 1999, **289**, 991–1002.
13 A. Hadfield, C. Shammas, G. Kryger, D. Ringe, G. A. Petsko, J. Ouyang and R. E. Viola, *Biochemistry*, 2001, **40**, 14475–14483.
14 W. E. Karsten and R. E. Viola, *Biochim. Biophys. Acta, Protein Struct. Mol. Enzymol.*, 1991, **1077**, 209–219.
15 R. J. Cox, J. S. Gibson and M. B. Mayo Martín, *ChemBioChem*, 2002, **3**, 874–886.
16 R. J. Cox, J. S. Gibson and A. T. Hadfield, *ChemBioChem*, 2005, **6**, 2255–2260.
17 A. Khan, J. Parrish, M. Fraser, W. Smith, P. Bartlett and M. James, *Biochemistry*, 1998, **37**, 16839–16845.
18 FlexX Docking Software, BioSolveIT GmbH, http://www.biosolveit.de/.
19 L. D. Freedman and G. O. Doak, *Chem. Rev.*, 1957, **57**, 479–523.
20 C. Baldock, J. B. Rafferty, S. E. Sedelnikova, P. J. Baker, A. R. Stuitje, A. R. Slabas, T. R. Hawkes and D. W. Rice, *Science*, 1996, **274**, 2107–2110.
21 C. W. Levy, A. Roujeinikova, S. Sedelnikova, P. J. Baker, A. R. Stuitje, A. R. Slabas, D. W. Rice and J. B. Rafferty, *Nature*, 1999, **398**, 383–384.
22 D. G. Gourley, A. W. Schüttelkopf, G. A. Leonard, J. Luba, L. W. Hardy, S. M. Beverley and W. N. Hunter, *Nat. Struct. Biol.*, 2001, **8**, 521–525.
23 J.-C. Jung and M. A. Avery, *Tetrahedron: Asymmetry*, 2006, **17**, 2479–2486.
24 L. D. Quin, *A Guide to Organophosphorus Chemistry*, Wiley Interscience, New York, 2000.
25 W. J. Murphy, *Organophosphorus Reagents*, Oxford University Press, Oxford, 2004.
26 R. Rodriguez, R. M. Adlington, S. J. Eade, M. W. Walter, J. E. Baldwin and J. E. Moses, *Tetrahedron*, 2007, **63**, 4500–4509.
27 R. J. Cohen, D. L. Fox, J. F. Eubank and R. N. Salvatore, *Tetrahedron Lett.*, 2003, **44**, 8617–8621.
28 W. Perkow, *Chem. Ber.*, 1954, **87**, 755–758.
29 W. Hoffmann, C. Simmons and J. Glunz, *J. Am. Chem. Soc.*, 1957, **79**, 3570–3575.
30 Z. Yoshida, S. Yoneda and T. Kawase, *Chem. Lett.*, 1975, **4**, 279–280.
31 S. Yoneda, T. Kawase and Z. Yoshida, *J. Org. Chem.*, 1978, **43**, 1980–1985.
32 R. Mayer, G. Hiller, M. Nitzschke and J. Jentzsch, *Angew. Chem., Int. Ed. Engl.*, 1963, **2**, 370–373.
33 R. A. Moore, W. E. Bocik and R. E. Viola, *Protein Expression Purif.*, 2002, **25**, 189.
34 H. Bisswanger, *Enzyme Kinetics; Principles and Methods*, Wiley-VCH, Weinheim, Germany, 2008.
35 The PyMOL Molecular Graphics System, Version 0.99, DeLano Scientific LLC, http://www.pymol.org/.
36 CORINA, Molecular Networks GmbH, http://www.molecular-networks.com.